Supporting Information

# Thermochromism and piezochromism of an atomically precise high-nuclearity silver cluster

Qiao-Qiao Sun,[a] Qian Li,[b] Hai-Yang Li,*[,a] Miao-Miao Zhang,[b] Meng-En Sun,[a] Si Li,[a] Zewei Quan,*[,b] Shuang-Quan Zang[a]

[a] Green Catalysis Center, and College of Chemistry, Zhengzhou University, Zhengzhou 450001 (China)

[b] Department of Chemistry, Academy for Advanced Interdisciplinary Studies, Shenzhen Engineering Research Center for Frontier Materials Synthesis at High Pressures, Southern University of Science and Technology (SUSTech), Shenzhen, Guangdong 518055, China

E-mail: quanzw@sustech.edu.cn； lihaiyang@zzu.edu.cn;

# Table of Contents

## Experimental section

**Materials and reagents**. All chemicals and solvents obtained from suppliers were used without further purification. All solvents were analytical grade reagent.

**Instrumentation**. Room temperature powder X-ray diffraction (PXRD) patterns of **1·4DMI** were collected at room temperature in air using an X' Pert PRO diffractometer (Cu-Kα). Temperature-dependent single-crystal UV-vis absorption spectra were recorded on a Craic Technologies microspectrophotometer. Crystals were placed on quartz slides under Krytox oil, and data were collected after optimization of the microspectrophotometer. Temperature-dependent PXRD patterns were recorded on a Rigaku XtaLAB PRO single-crystal X-ray diffractometer using the powder tool (Cu-Kα radiation). Thermogravimetric (TG) analyses of the as-synthesized nanoclusters were performed on an SDT 2960 thermal analyzer from room temperature to 400 °C at a heating rate of 10 °C/min in a nitrogen atmosphere.

**High pressure sample loading**. High-pressure experiments were performed using a diamond anvil cell (DAC). A pair of 0.4 mm diamond culets was equipped in the DAC to generate high-pressure conditions. The sample chamber contained a 150 μm-diameter aperture, which was drilled in the center of a preindented T301 gasket that was ~ 60 μm thick. The sample was loaded into the sample holder with silicon oil (Aldrich, ∼150 mPa·s) as the pressure transmitting medium (PTM) and ruby balls were used to calibrate the pressure value during compression. All the experiments were performed at room temperature.

**High pressure UV−vis absorption experiments.** High-pressure absorption experiments were carried out on an Ocean Optics QE65000 spectrometer with the transmittance method. Before detection, the transmission spectrum of silicon oil was subtracted as the background.

**High pressure Raman experiments.** High-pressure Raman spectra were measured using a commercial HORIBA LabRAM HR Evolution Raman spectrometer.

**Single crystal analysis**. Single-crystal X-ray diffraction measurements of **1·4DMI** were performed on a Rigaku XtaLAB PRO diffractometer with Cu-Kα radiation at 100, 150 and 200 K. Data collection and reduction were performed using the program CrysAlisPro.[1] All the structures were solved with direct methods (*SHELXS*)[2] and refined by full-matrix least squares on $F^2$ using *OLEX2*,[3] which utilizes the *SHELXL*-2015 module.[4] All nonhydrogen atoms were refined anisotropically. Hydrogen atoms were placed in calculated positions that were refined using idealized geometries that assigned fixed isotropic displacement parameters. Imposed restraints in least-squares refinement of each structure were commented on in the corresponding crystallographic information framework (CIF) files. Thus, only a general description of the structural refinement strategy is presented here. A satisfactory disorder model for the solvent molecules in **1·4DMI** was not found; therefore, the *OLEX2* Solvent Mask routine (*PLATON/SQUEEZE*)[5] was used to mask the disordered density. The relevant crystallographic data and structure-refinement details are shown in Table S2.

**General procedures:**

**Synthesis of silver *p*-fluorinated phenylthiol (Precursor)**. $AgNO_3$ (170 mg, 1.00 mmol) was dissolved in 20 mL acetonitrile, and then *p*-fluorothiophenol (108 $\mu$L, 1.00 mmol) was added. After stirring for one minute, the color of the solution immediately changed from colorless to a faint yellow turbidity. The solution was filtered and the faint yellow precipitate (precursor) was collected with a yield of 60% (based on Ag).

**Synthesis of 1·4DMI.** The precursor (10 mg, 0.0425 mmol) was added to a mixed solution of 1 mL 1,3-dimethyl-2-imidazolidinone (DMI) and 2 mL trichloromethane ($CHCl_3$), and then 1,3-diphenylphosphine propane (15 mg, 0.0364 mmol) was added to make the solution clear. After stirring for an extended time period, the color of the solution became colorless. Then, silver benzoate (3 mg, 0.0130 mmol) was added, and the solution remained colorless. Finally, 10 drops of carbon disulfide were added to the solution, and the solution immediately turned yellow and clear. The resultant solution was allowed to evaporate slowly in darkness at room temperature for three days to give an orange-red strip of crystals with a yield of 50% (based on Ag). Elemental analysis (%) for $C_{398}H_{340}N_8S_{43}P_{12}Ag_{50}F_{36}O_4$ (100 K), found (calculated): C, 36.26 (36.41); H, 2.58 (2.61); N, 0.82 (0.85).

## Supplementary Figure

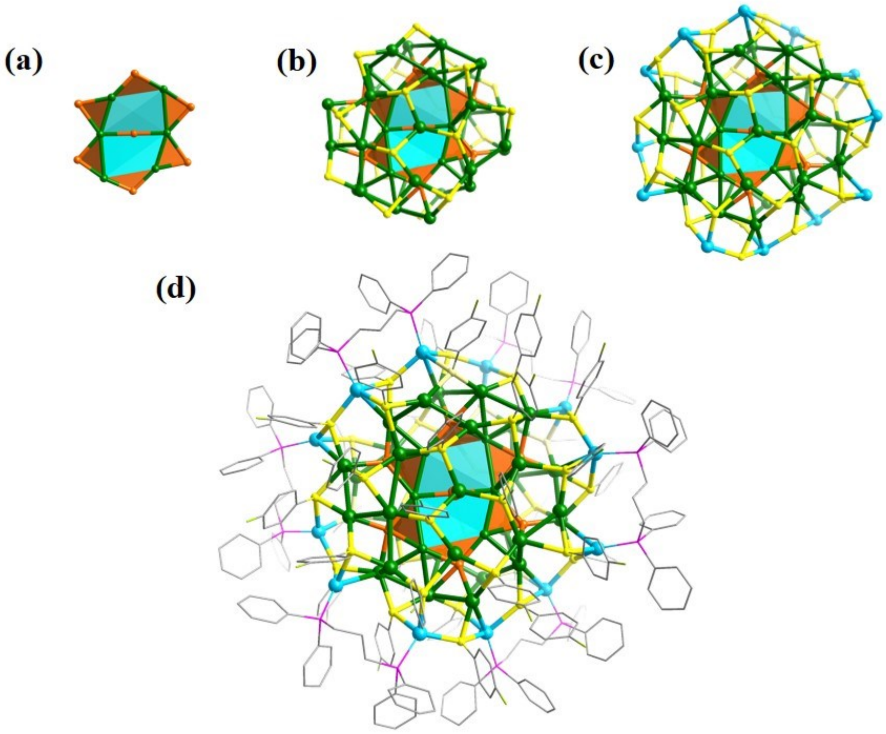

**Figure S1.** The ball and stick model diagrams of **1** ([$Ag_{50}S_7(SPhF)_{36}(dppp)_6$]) except the peripheral ligands (dppp = 1,3-diphenylphosphine propane). (a) The $Ag_6S_7$ core in the inner part of **1**, the $Ag_6S_7$ core contains six silver (I) ions and seven sulfide ions, which can be depicted as six triangles and two distorted tetrahedrons. (b) The $Ag_6S_7$ core encapsulated in an $Ag_{32}S_{22}$ shell. (c) The $Ag_6S_7@Ag_{32}S_{22}$ core-shell structure surrounded by an $Ag_{12}S_{14}$ motif around the middle. (d) The overall structure of **1**. Color labels: green and sky blue, Ag; yellow and orange, S (thiolate) and $S^{2-}$; bright green, F; purple, P; and gray, C. All H atoms are omitted for clarity.

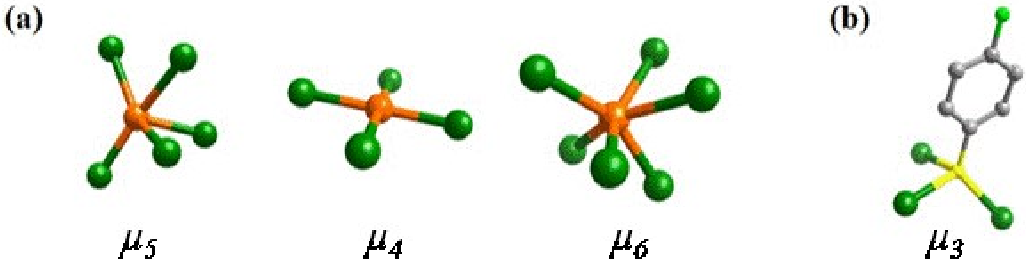

**Figure S2.** (a) Coordination pattern diagram of $S^{2-}$. (b) Coordination pattern diagram of the $FPhS^-$ ligand. Color labels: green, Ag; orange, $S^{2-}$; yellow, S (derived from FPhSH); bright green, F; and gray, C.

.

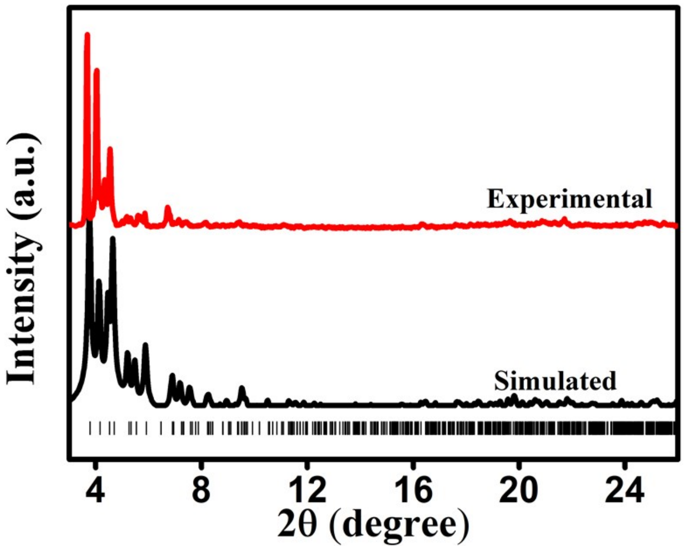

**Figure S3.** PXRD spectra of **1·4DMI.**

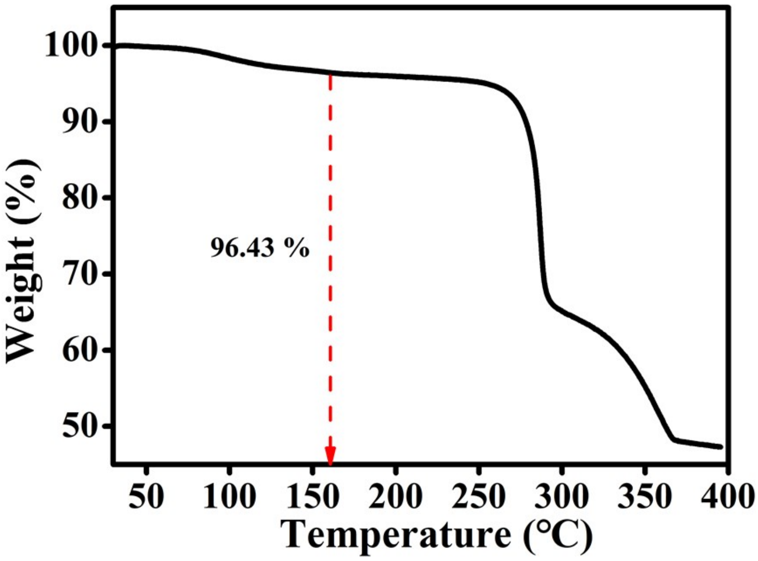

**Figure S4.** The thermal gravimetric curve of **1·4DMI.** The weight loss (3.57%) from approximately 95 °C to 160 °C can be ascribed to the removal of the 4 DMI (1,3-dimethyl-2-imidazolidinone) solvent molecules (calculated as 3.52%).

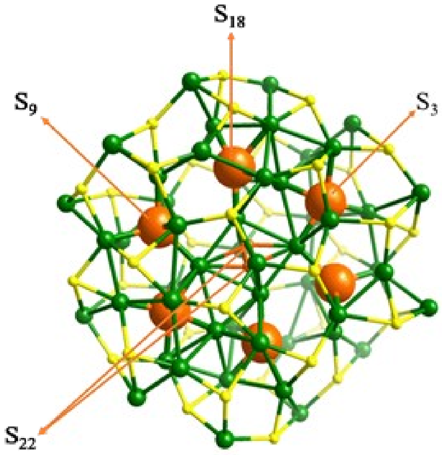

**Symmetry code:** $^{1}1 - x, 1 - y, - z$

**Figure S5.** The overall structure of **1** while ignoring the peripheral ligands. The large orange spheres represent $S^{2-}$. Color labels: green sphere, Ag and yellow and orange sphere, S (thiolate) and $S^{2-}$, respectively. Table S3 shows the changes in the selected bond lengths of **1** (two $S_{22}$ atoms show the disorder of the sulfur atom) at different temperatures.

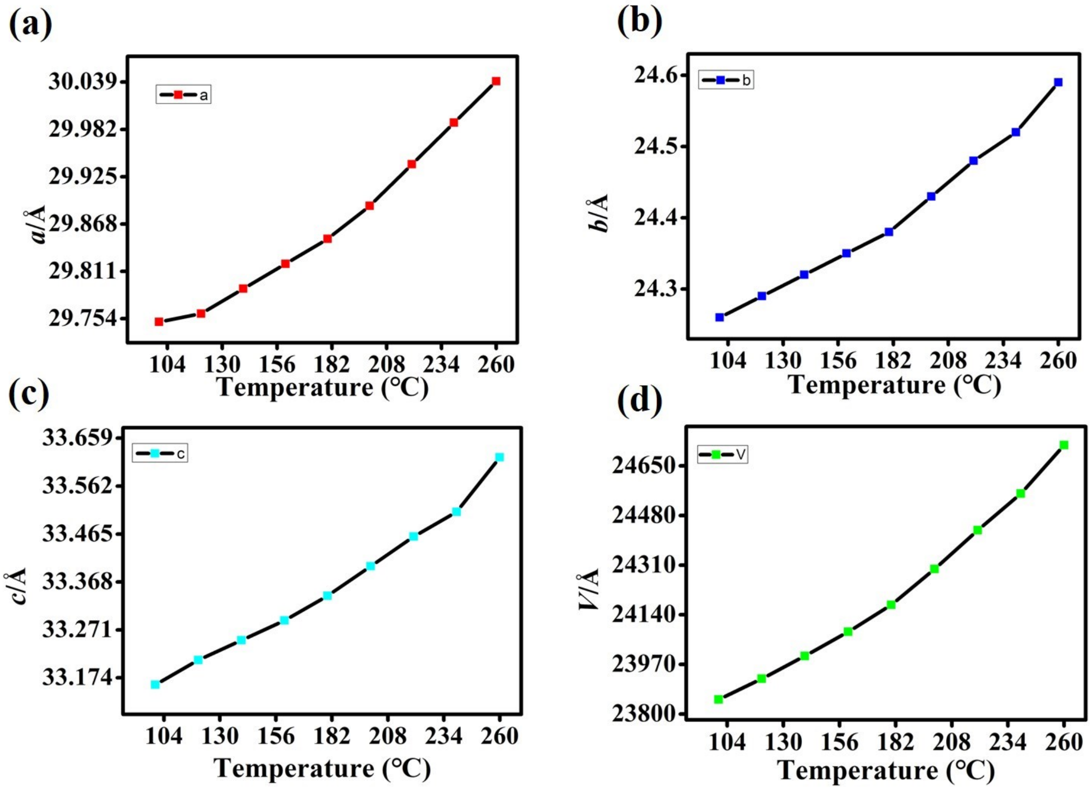

**Figure S6.** Variation in the unit-cell parameters of (a) a, (b) b, and (c) c, and the (d) volume of **1·4DMI** versus temperature.

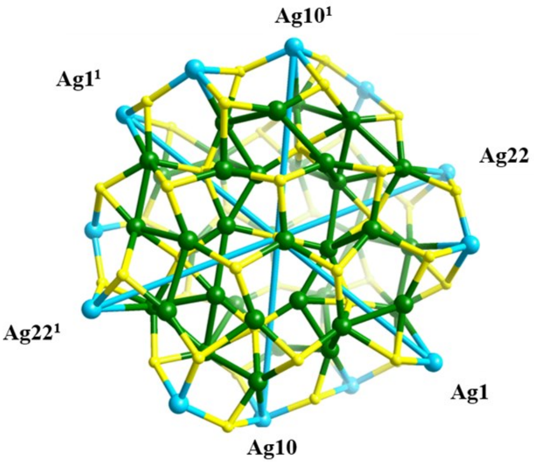

**Symmetry code:** ¹1 - *x*, 1 - *y*, - *z*

**Figure S7.** Distances between Ag1 and Ag1[1], Ag10 and Ag10[1], Ag22 and Ag22[1]. The detailed data are in Table S5. Color labels: green and sky blue spheres, Ag; yellow spheres, S (thiolate) and $S^{2-}$.

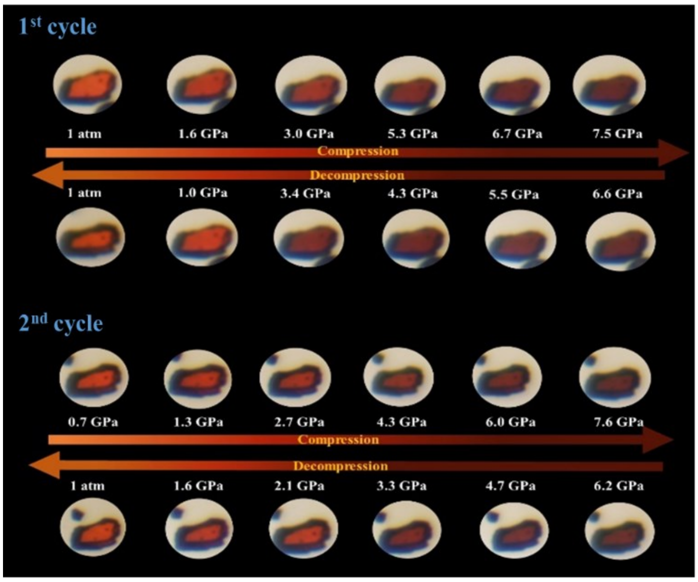

**Figure S8**. Optical images of the **1** under ambient light during two consecutive compression-decompression cycles.

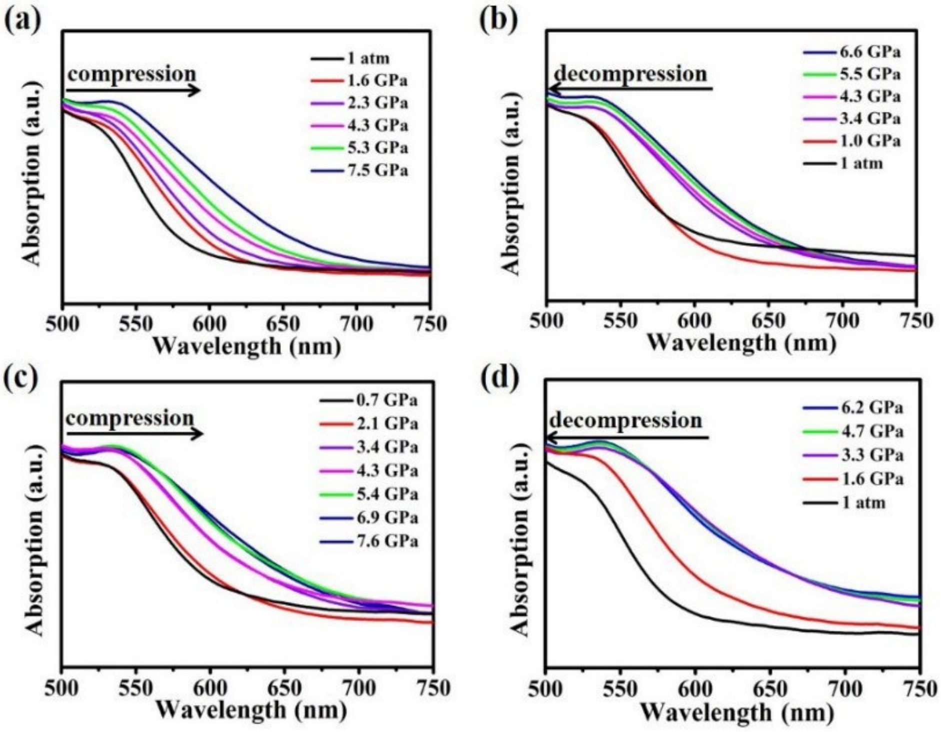

**Figure S9.** (a - d) *In situ* UV-vis absorption spectra of **1** during two consecutive compression-decompression cycles..

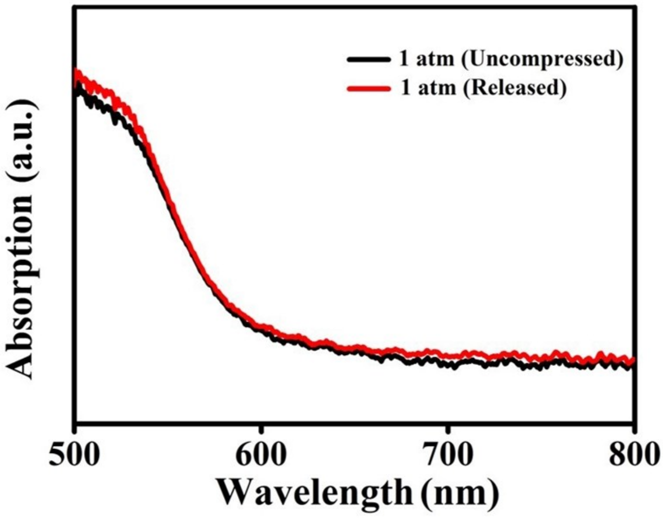

**Figure S10.** UV-vis absorption spectra before compression and release.

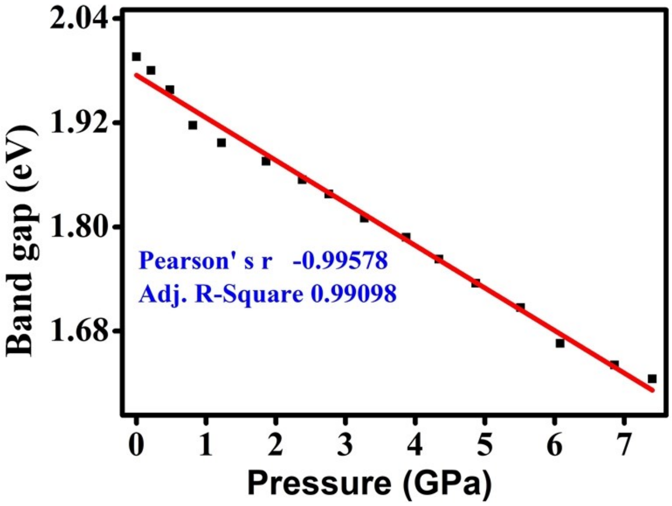

**Figure S11.** Indirect band gap evolution of **1** as a function of pressure calculated from Tauc plots.

1st compression

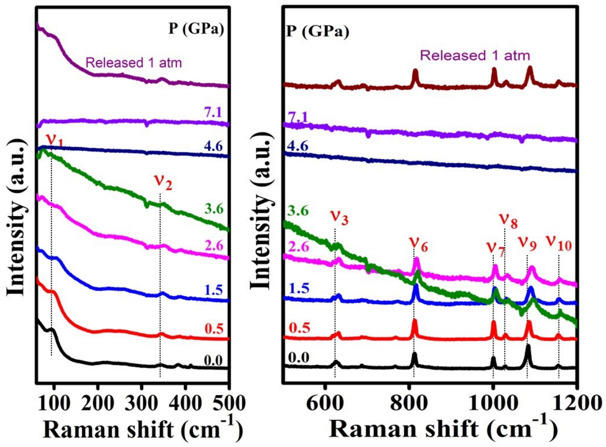

2nd compression

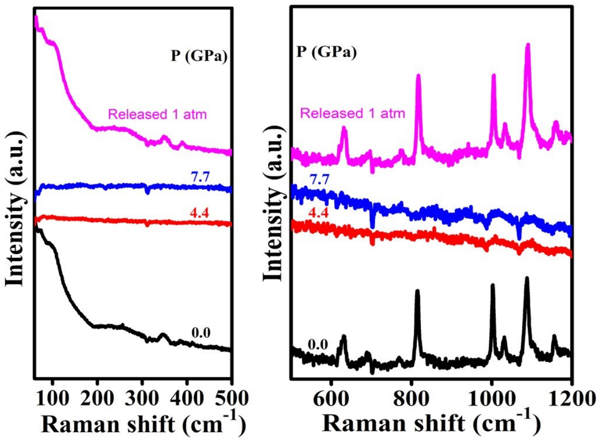

**Figure S12.** Raman spectra of **1** during two consecutive compression-decompression cycles. Due to the weak vibration bands, the $\nu_4$ and $\nu_5$ vibration modes are not shown in the diagram.

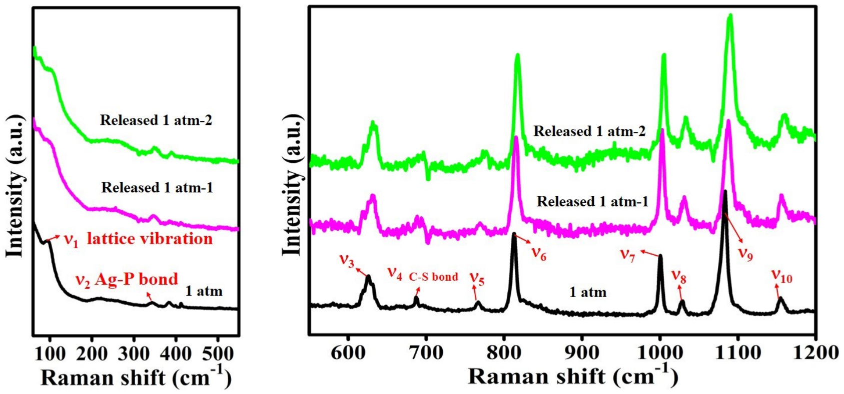

**Figure S13.** Raman spectra of **1** before and after two cycles of compression. The vibrations mode $\nu_1$ at about 95 cm$^{-1}$ is associated with the lattice vibration, the vibration band $\nu_2$ at about 343 cm$^{-1}$ is recognized as a characteristic Ag−P vibration peak. The $\nu_3$ vibration mode (about 626 cm$^{-1}$) is associated with benzene ring deformation motion and the $\nu_4$ (about 687 cm$^{-1}$) is C−S bond vibrational mode. The $\nu_5$ vibration mode (about 765 cm$^{-1}$), the strong vibration band $\nu_6$ (about 813 cm$^{-1}$) and $\nu_{10}$ (about 1154 cm$^{-1}$) are recognized as a characteristic C−H bending vibrations peaks of benzene. The $\nu_7$ vibration mode (about 1000 cm$^{-1}$) is associated with benzene ring breathing vibration，the $\nu_8$ vibration mode (about 1030 cm$^{-1}$) and $\nu_9$ (about 1080 cm$^{-1}$) vibration band are associated with C−C benzene ring stretching.

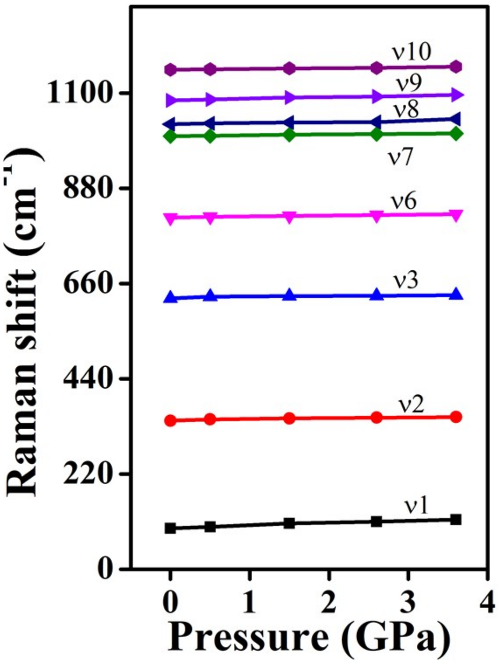

**Figure S14.** Raman shift of **1** as a function of pressure.

**Table S1.** Selected bond lengths (Å) in **1** at 100 K.

| **Atom-Atom** | **Bond length/Å** | **Atom-Atom** | **Bond length/Å** |
|---|---|---|---|
| Ag1-Ag2 | 3.1991(10) | Ag1-S1 | 2.569(2) |
| Ag1-Ag15 | 3.3634(10) | Ag1-S2 | 2.496(2) |
| Ag1-P1 | 2.412(2) | Ag2-Ag15 | 3.1192(12) |
| Ag2- Ag23 | 2.9666(10) | Ag2-S2 | 2.565(2) |
| Ag2-S7 | 2.781(3) | Ag2-S9 | 2.589(2) |
| Ag2-S11 | 2.568(2) | Ag3-Ag21 | 3.0863(10) |
| Ag3-S2 | 2.615(2) | Ag3-S4 | 2.703(2) |
| Ag3-S15 | 2.538(2) | Ag3-P4 | 2.432(3) |
| Ag4-Ag15 | 2.9225(10) | Ag4-Ag21 | 2.8895(11) |
| Ag4-Ag25 | 2.9453(17) | Ag4-S1 | 2.763(2) |
| Ag4-S5 | 2.513(2) | Ag4-S9 | 2.694(2) |
| Ag4-S16 | 2.599(3) | Ag5-Ag26$^1$ | 3.3485(17) |
| Ag5-Ag26 | 3.0299(17) | Ag5-S10 | 2.639(3) |
| Ag5-S16 | 2.587(2) | Ag5-S17 | 2.632(2) |
| Ag5-S22$^1$ | 2.644(5) | Ag5-S22$^1$ | 2.644(5) |
| Ag6-Ag24 | 3.1081(13) | Ag6-Ag27$^1$ | 3.096(7) |
| Ag6-S3 | 2.668(3) | Ag6-S8 | 2.566(3) |
| Ag6-S16 | 2.506(2) | Ag6-S21 | 2.692(3) |
| Ag7-Ag12$^1$ | 3.0214(12) | Ag7-Ag18$^1$ | 3.1574(12) |
| Ag7-Ag20 | 3.1739(11) | Ag7-Ag22 | 3.1424(10) |
| Ag7-S12$^1$ | 2.621(2) | Ag7-S19 | 2.537(3) |
| Ag8-Ag23 | 3.1724(13) | Ag8-S11 | 2.704(3) |
| Ag8-S12 | 2.560(3) | Ag8-S21 | 2.591(3) |
| Ag8-P5 | 2.450(3) | Ag9-Ag11 | 3.3281(11) |
| Ag9-Ag18 | 3.1060(11) | Ag9-Ag23 | 2.9859(12) |
| Ag9-Ag24 | 3.0622(11) | Ag9-S3 | 2.638(3) |
| Ag9-S7 | 2.501(2) | Ag9-S17$^1$ | 2.501(3) |
| Ag10-S14 | 2.600(2) | Ag10-S20 | 2.673(3) |
| Ag10-P2 | 2.432(3) | Ag11-Ag21 | 3.3165(11) |
| Ag11-Ag24 | 3.3734(16) | Ag11-Ag25 | 3.0666(17) |
| Ag11-S7 | 2.553(2) | Ag11-S9 | 2.637(3) |
| Ag11-S10$^1$ | 2.508(2) | Ag11-S15 | 2.889(3) |
| Ag12-Ag16$^1$ | 3.0466(13) | Ag12-Ag17 | 2.9708(12) |
| Ag12-Ag18 | 3.0020(10) | Ag12-Ag20$^1$ | 2.9526(14) |
| Ag12-Ag24 | 3.1628(16) | Ag12-Ag26$^1$ | 2.7739(15) |
| Ag12-S3 | 2.374(2) | Ag12-S18 | 2.399(3) |
| Ag13-Ag16 | 3.2801(12) | Ag13-Ag20 | 3.2050(13) |
| Ag13-S5 | 2.565(3) | Ag13-S18$^1$ | 2.560(3) |
| Ag13-S20 | 2.436(3) | Ag14-Ag17$^1$ | 3.0712(11) |
| Ag14-Ag21 | 3.3367(13) | Ag14-S14 | 2.436(2) |
| Ag14-S15 | 2.415(2) | Ag15-S1 | 2.438(2) |
| Ag15-S9 | 2.967(3) | Ag15-S21 | 2.404(3) |

| | | | |
|---|---|---|---|
| Ag16-Ag26 | 3.3562(16) | Ag16-S5 | 2.486(2) |
| Ag16-S13 | 2.832(3) | Ag16-S17 | 2.467(2) |
| Ag16-S18$^1$ | 2.913(4) | Ag17-Ag20$^1$ | 2.9837(12) |
| Ag17-Ag26$^1$ | 3.2160(18) | Ag17-S8 | 2.457(3) |
| Ag17-S10 | 2.486(2) | Ag17-S18 | 2.650(3) |
| Ag18-Ag28$^1$ | 2.819(6) | Ag18-S6 | 2.402(2) |
| Ag18-S13$^1$ | 2.411(3) | Ag19-S13 | 2.590(3) |
| Ag19-S19 | 2.691(4) | Ag19-S20 | 2.587(2) |
| Ag19-P6 | 2.456(3) | Ag20-S14 | 2.568(3) |
| Ag20-S18$^1$ | 2.632(3) | Ag20-S19 | 2.441(3) |
| Ag21-Ag25 | 2.7246(17) | Ag21-S4 | 2.405(2) |
| Ag21-S9 | 2.406(3) | Ag22-S6$^1$ | 2.570(3) |
| Ag22-S12$^1$ | 2.408(3) | Ag22-P3 | 2.380(3) |
| Ag23-Ag27$^1$ | 3.065(8) | Ag23-S3 | 2.455(2) |
| Ag23-S6 | 2.785(2) | Ag23-S11 | 2.412(2) |
| Ag24-S3 | 2.534(2) | Ag24-S9 | 2.647(3) |
| Ag25-S9 | 2.414(2) | Ag25-S18$^1$ | 2.358(3) |
| Ag25-S22 | 2.694(5) | Ag26-S18$^1$ | 2.397(3) |
| Ag24-S22 | 2.584(4) | Ag24-S22$^1$ | 2.343(4) |

**Symmetry code:** $^1 1 - x, 1 - y, - z$

**Table S2.** Crystal data and structure refinements for **1** at 100 K, 150 K and 200 K.

| **Temperature/K** | **100** | **150** | **200** |
|---|---|---|---|
| **Empirical formula** | $C_{398}H_{340}N_8S_{43}P_{12}Ag_{50}F_{36}O_4$ | $C_{398}H_{340}N_8S_{43}P_{12}Ag_{50}F_{36}O_4$ | $C_{378}H_{300}Ag_{50}F_{36}P_{12}S_{43}$ |
| **Formula weight** | 13126.48 | 13126.48 | 12669.88 |
| **Crystal system** | monoclinic | monoclinic | monoclinic |
| **Space group** | $P2_1/c$ | $P2_1/c$ | $P2_1/c$ |
| **Z** | 2 | 2 | 2 |
| **a/Å** | 30.0312(2) | 30.0586(2) | 30.1143(2) |
| **b/Å** | 24.2172(2) | 24.3044(2) | 24.4007(2) |
| **c/Å** | 42.6434(5) | 42.7656(5) | 42.8993(4) |
| **α/°** | 90 | 90 | 90 |
| **β/°** | 129.0600(10) | 129.0630(10) | 129.0550(10) |
| **γ/°** | 90 | 90 | 90 |
| **Volume/Å$^3$** | 24081.4(5) | 24258.5(5) | 24478.8(4) |
| ***ρcalcg/cm$^3$*** | 1.810 | 1.797 | 1.719 |
| **2*θ* range for data collection/°** | 4.696 to 148.556 | 4.684 to 148.406 | 3.778 to 148.292 |
| **F(000)** | 12716.0 | 12716.0 | 12220.0 |
| ***μ*/mm$^{-1}$** | 18.494 | 18.359 | 18.158 |
| **Reflections collected** | 149168 | 149132 | 151285 |
| **Independent reflections** | 47496 | 47895 | 48344 |
| **Completeness** | 97 | 97 | 97 |
| ***R*(int)** | 0.0794 | 0.0485 | 0.0472 |
| **Goodness-of-fit on F$^2$** | 1.121 | 1.058 | 1.055 |
| **$R_1$ $^a$ [$I > 2\sigma(I)$]** | 0.0889 | 0.0782 | 0.0902 |
| **$wR_2$ $^b$** | 0.2518 | 0.2146 | 0.2765 |
| **$R_1$$^a$ [all data]** | 0.0988 | 0.0927 | 0.1095 |
| **$wR_2$ $^b$** | 0.2648 | 0.2272 | 0.2973 |
| **CCDC number** | 1992657 | 1992658 | 1992659 |

$R_1 = \sum||F_o|-|F_c||\sum/|F_o|$. $wR_2 = [\sum w(F_o^2 - F_c^2)^2/\sum w(F_o^2)^2]^{1/2}$

**Table S3.** Selected bond lengths (Å) in **1** at different temperature.

| **Atom-Atom** | **100 K** | **150 K** | **200 K** |
|---|---|---|---|
| Ag12-Ag24 | 3.1628(16) | 3.1800(17) | 3.198(2) |
| Ag4-S9 | 2.694(2) | 2.678(2) | 2.660(3) |
| Ag24-S9 | 2.647(3) | 2.659(3) | 2.676(4) |
| Ag2-S9 | 2.589(2) | 2.589(2) | 2.601(2) |
| Ag6-S3 | 2.668(3) | 2.669(2) | 2.677(3) |
| Ag23-S3 | 2.455(2) | 2.461(2) | 2.476(3) |
| Ag25-S18$^1$ | 2.358(3) | 2.354(3) | 2.344(4) |
| Ag9-S3 | 2.638(3) | 2.640(3) | 2.640(3) |
| Ag13-S18$^1$ | 2.560(3) | 2.567(3) | 2.575(3) |
| Ag12-S18 | 2.399(3) | 2.382(3) | 2.363(3) |
| Ag17-S18 | 2.650(3) | 2.648(3) | 2.644(3) |
| Ag24-S22 | 2.584(4) | 2.339(5) | 2.335(6) |
| Ag12-Ag20$^1$ | 2.9526(14) | 2.9601(18) | 2.946(2) |
| Ag17$^1$-Ag14 | 3.0712(11) | 3.0815(13) | 3.0923(16) |
| Ag20$^1$-Ag17 | 2.9837(12) | 2.9767(13) | 3.0923(16) |
| Ag23-Ag27$^1$ | 3.065(8) | 3.080(5) | 3.097(4) |
| Ag12-Ag18 | 3.0020(10) | 3.0135(15) | 3.0228(17) |

| | | | |
|---|---|---|---|
| Ag10-Ag13 | 3.1686(13) | 3.1896(13) | 3.2016(18) |
| Ag5-S10 | 2.639(3) | 2.642(3) | 2.643(3) |
| Ag11-S10$^{1}$ | 2.508(2) | 2.516(2) | 2.515(3) |
| Ag17-S10 | 2.486(2) | 2.479(2) | 2.471(3) |
| Ag3-S15 | 2.538(2) | 2.542(2) | 2.550(3) |
| Ag3-P4 | 2.432(3) | 2.435(3) | 2.436(3) |
| Ag1-P1 | 2.412(2) | 2.411(2) | 2.408(3) |
| Ag8-P5 | 2.450(3) | 2.455(3) | 2.460(3) |
| Ag22-P3 | 2.380(3) | 2.379(3) | 2.381(3) |
| Ag19-P6 | 2.456(3) | 2.457(3) | 2.450(3) |
| Ag10-P2 | 2.432(3) | 2.434(3) | 2.431(3) |

**Table S4.** The lattice distance of different axis at different temperature.

| | **100 K** | **150 K** | **200 K** |
|---|---|---|---|
| ***a*** | 30.03(2) Å | 30.06(2) Å | 30.11(2) Å |
| ***b*** | 24.22(2) Å | 24.30(2) Å | 24.40(2) Å |
| ***c*** | 42. 64(2)Å | 42.77(2) Å | 42. 90(4) Å |

**Table S5.** Selected bond length variations of **1** at different temperature.

| | **100 K** | **150 K** | **200 K** |
|---|---|---|---|
| Ag1-Ag1$^{1}$ | 18.078(2) Å | 18.094(2) Å | 18.120(2) Å |
| Ag10-Ag10$^{1}$ | 17.100(2) Å | 17.152(2) Å | 17.209(2) Å |
| Ag22-Ag22$^{1}$ | 17.732(2) Å | 17.771(2) Å | 17.809(2) Å |

**Symmetry code:** $^{1}$1 - *x*, 1 - *y*, - *z*

## References

[1] CrysAlisPro 2012, Agilent Technologies. Version 1.171.36.31

[2] G. M. Sheldrick, *Acta Cryst. A* **2008**, *64*, 112.

[3] O. V. Dolomanov, L. J. Bourhis, R. J. Gildea, J. A.-K. Howard, H. Puschmann, *J. Appl. Cryst.* **2009**, *42*, 339-341.

[4] G. M. Sheldrick, *Acta Cryst. C* **2015**, *71*, 3.

[5] A. L. Spek, *Acta Cryst. C* **2015**, *71*, 9.